Zuse Institute Berlin

Takustr. 7
14195 Berlin
Germany

FEDA SEBLANY, ULRIKE HOMBERG, ERIC VINCENS,
PAUL WINKLER, KARL JOSEF WITT

Merging criteria for defining pores and constrictions in numerical packing of spheres

Has appeared in a slightly different version in: Granular Matter (2018) 20:37, Springer, https://doi.org/10.1007/s10035-018-0808-z.

ZIB Report 18-25 (June 2018)

Zuse Institute Berlin
Takustr. 7
14195 Berlin
Germany

Telephone: +49 30-84185-0
Telefax: +49 30-84185-125

E-mail: bibliothek@zib.de
URL: http://www.zib.de

ZIB-Report (Print) ISSN 1438-0064
ZIB-Report (Internet) ISSN 2192-7782

Merging criteria for defining pores and constrictions in numerical packing of spheres

Feda Seblany[1] · **Ulrike Homberg**[2] · **Eric Vincens**[1] · **Paul Winkler**[3] · **Karl Josef Witt**[3]

Abstract The void space of granular materials is generally divided into larger local volumes denoted as pores and throats connecting pores. The smallest section in a throat is usually denoted as constriction. A correct description of pores and constrictions may help to understand the processes related to the transport of fluid or fine particles through granular materials, or to build models of imbibition for unsaturated granular media. In the case of numerical granular materials involving packings of spheres, different methods can be used to compute the pore space properties. However, these methods generally induce an over-segmentation of the pore network and a merging step is usually applied to mitigate such undesirable artifacts even if a precise delineation of a pore is somewhat subjective. This study provides a comparison between different merging criteria for pores in packing of spheres and a discussion about their implication on both the pore size distribution and the constriction size distribution of the material. A correspondence between these merging techniques is eventually proposed as a guide for the user.

Keywords Delaunay tessellation · Voronoï graph · Void space · Granular materials

1 Introduction

A granular medium includes a set of large volumes of voids between solid particles (pores) connected by throats. The narrowest sections in these throats are generally denoted as constrictions. Pores and constrictions constitute a partition of the void space helpful to define respectively its morphology and its topology [28, 45]. Such a partition can also help to build imbibition models for unsaturated materials [16,23], models for the coefficient of permeability [7,8] for fluid-calculation, or geometrical filtration models for studying the migration of particles through granular media [21,32,34,35].

There are different techniques for pore space characterization: through experiments [15,19,40,42,46], using analytical approaches [22,29,36] or numerical approaches [17,26,28]. To overcome some limitations associated with experimental methods, the Discrete Element Method (DEM) (among others [10]) can be helpful to draw some main tendencies for packings of spheres with a given grading and density. The pore space of such a packing can be extracted by combining the DEM with spatial partitioning techniques: the Delaunay tessellation [2,28,41] or its dual structure, the Voronoï diagram [14,30,47] among others.

In the Delaunay tessellation, the primary definition for a local pore is the Delaunay cell, i.e. a tetrahedron which vertices are located at the centers of spherical particles. Constrictions are found on the four faces of each tetrahedron and a definition for them is chosen as the largest empty discs that can be inscribed between the three particle vertices of a tetrahedron face [2,28] (Fig. 1). Eventually, the inscribed void sphere between the four particles, vertices of a Delaunay cell is computed and be considered as a characteristic of the morphology of that cell. Obviously, the derived partition of the void space is somehow artificial since a Delaunay cell is merely related to the underlying mathematical process of finding the three closest neighbors of a given particle to generate a tetrahedron.

[1]Université de Lyon, Ecole centrale de Lyon, LTDS, UMR CNRS 5513, 36 avenue Guy de Collongue, 69134 Ecully, France

[2]Zuse Institute Berlin, Department Visual Data Analysis, Takustr. 7, 14195 Berlin-Dahlem, Germany

[3]Bauhaus-Universität Weimar, Chair of Geotechnical Engineering, Coudraystraße 11c, 99423 Weimar, Germany

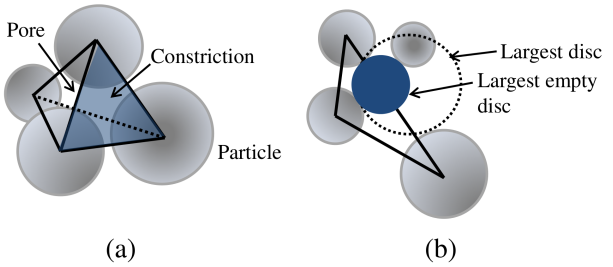

Fig. 1 **(a)**: Tetrahedron built from the centers of four neighboring spheres; **(b)**: Definition of a constriction: the largest disc included in the void space for a given face

While the Delaunay tetrahedra constitute volumetric entities that cover pores or parts of pores, a Voronoï graph can complement the definition of the pore structures. Due to the duality of Delaunay and Voronoï decompositions, the Voronoï nodes should correspond to the centers of the inscribed void spheres of the Delaunay tetrahedra and their distance to the surrounding solid spheres to the radius of these inscribed void spheres. When applying a Voronoï computation that is based on the Euclidean distance to the solid spheres as described by Lindow et al. [20], the edges between the Voronoï nodes are curved and run along the maximal distance to the surrounding solid spheres. Then, they describe the median path joining pore centers. The centers of constrictions are located where the distance to the surrounding spheres is minimal along the edge. In terms of duality, this is where the edges cut the common facet of the tetrahedra of the connecting Voronoï nodes and, thus, correspond to the constrictions found in the Delaunay tessellation (Fig. 2).

Even if the equivalence of results for the constriction size distribution (CSD) extracted from a Delaunay tessellation and a Voronoï graph has been proven in the past for a packing of spheres [44], the question arises whether an excessive artificial partition of the void space is generated by both mathematical techniques and how to handle it.

Indeed, using a Delaunay tessellation, Al-Raoush et al. [2] found that the inscribed void sphere confined in each tetrahedron is not necessarily entirely included inside that tetrahedron, and two inscribed void spheres attached to these two neighboring tetrahedra may overlap. It signifies that the opening size between two adjacent tetrahedra may be high enough to indicate a strong interconnection between them. As a result, the tetrahedral tessellation would tend to abusively subdivide a complete pore structure into zones.

For the same reason, Homberg et al. [17] considered that a merge between two adjacent pores may be required when the size of the constriction linking these pores is very close to the smallest pore size (case where the Voronoï approach is used to derive the void space properties). In fact, in such a case, pores are interconnected and seem to belong to a single entity. Figure 3 illustrates a case where two adjacent pores (hatched and shaded area) are going to be merged.

Because different techniques may lead to different pore structures and, as a consequence, to a different set of pore and constriction sizes, this study aims to better understand the implications of using a given technique for merging pores on the properties of the poral space in packing of spheres. The problem that arises here is that no definite poral structure can be derived for a packing since the boundaries of a so-called pore is vague by nature. Within these limits, this paper tries to draw some advantages and limits of two techniques for merging pores. The influence of the proposed criteria for merging on the pore structures is also addressed and, as a guide for the user, a correspondence between the criteria associated to both techniques for merging pores is given.

2 Generation of numerical samples

The open-source code Yade-DEM [39] was used here to generate numerical samples composed of spheres. In this DEM code, the contacts between particles are deformable while the particles are considered as infinitely rigid bodies [10].

Two gradings are studied: a narrowly graded material (UG) and a gap-graded material (GG). The former grading is the one studied in previous studies [28,38], ranging from $3mm$ to $12mm$ as shown in Figure 4a, with a coefficient of uniformity (C_u) equal to 1.7. The coefficient of uniformity measures the extent of particle diameters and is defined as the ratio of the diameter corresponding to 60% finer by weight to the diameter corresponding to 10% finer by weight. The latter grading is the one studied by Reboul et al. [29] and is given in Figure 4b. The minimum and maximum diameters (D_0 and D_{100}) for this material are respectively equal to $0.7mm$ and $10mm$, and C_u is equal to 3.6. Since different techniques for the sample creation may lead to different structures for the packing [4,31], a deposit under gravity of particles, which is a technique that reflects the process used in actual experiments, is preferred.

To create the sample, a loose cloud of spheres with a prescribed particle size distribution is initially generated in a box having a horizontal size equal to that of the final sample but with a larger vertical size (about twice as more as the horizontal size). The base of the box is a square of $40mm$ width (approximately $4D_{100}$). The lateral boundaries of the box are associated to periodic conditions in order to avoid wall effects in the final

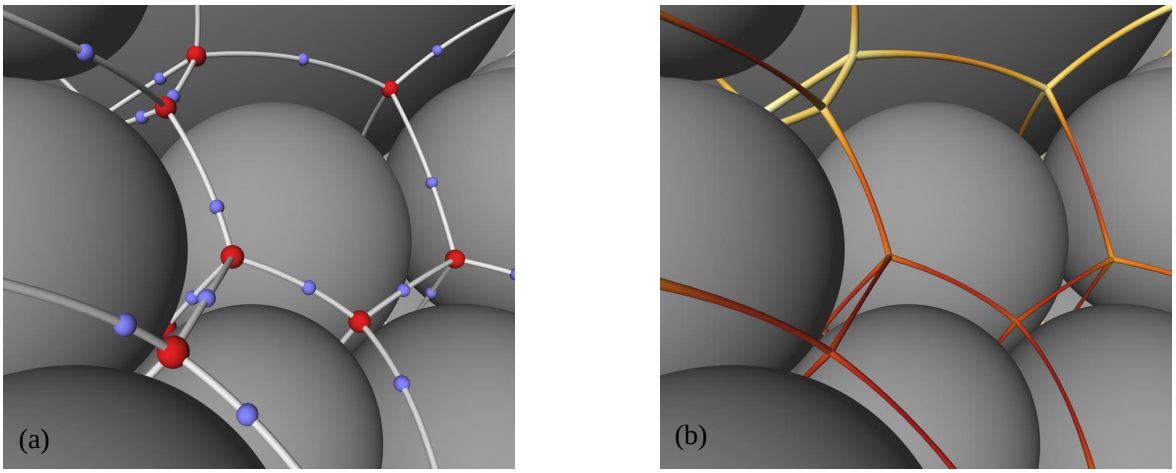

Fig. 2 Detail of a Voronoï graph (GGD); **(a)**: red spheres at crossing indicate the centers of pores, while the blue spheres represent the centers of constrictions on the edges; **(b)**: The diameter is color-coded along the edges with yellow (large) to red (small)

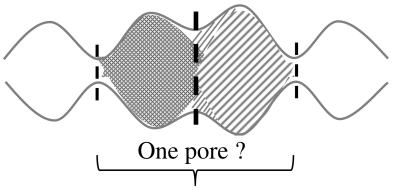

Fig. 3 Scheme of a typical case encountered during pore merging

samples [1,27]. If a sphere overlaps any other existing spheres, another position is attributed to this sphere.

After this stage of particle generation, the packing is subjected to gravity which induces the spheres to fall freely in the box according to Newton's laws. Interactions between particles may occur as particles collide. The process is ended when all particles reach a quasi-static equilibrium state. The equilibrium is supposed to have been found when the unbalanced forces (mean resultant forces at contact divided by the mean contact force over the sample) goes below 0.05.

The contact between particles and that between particle and the bottom wall of the sample box (this wall is ruled as a particle with an infinite radius) is characterized by an elastic-frictional model. It includes a normal and a tangential stiffness (respectively K_n and K_t) and tangential forces are limited by the Coulomb criterion characterized by a contact friction coefficient (μ).

In this study, particle density is taken equal to the one of glass beads, and typical values for K_n and K_t of such materials are chosen. For the specific contacts between a particle and the bottom wall of the box, the contact friction coefficient (μ) is set to 0. Dissipation in the system is introduced by means of a global damping (α) proportional to the acceleration forces [10].

In the case of UG material, 650 particles have been used while for GG material, packings with 25000 particles were generated to obtain representative statistical data. For each grading, two samples are generated corresponding to the loosest state (respectively UGL and GGL) and to the densest state (respectively UGD and GGD). The inter-particle friction coefficient is set to 0.3 which is approximately equal to the value obtained by experimental test on spherical glass beads [3]. The resulting maximum porosities for UGL and GGL match the targeted values obtained through experiments by Biarez and Hicher [6], for the same coefficient of uniformity and the same particle aspect ratio of 1 (difference between the largest dimension and the smallest dimension of a particle). These authors used the ASTM standard to determine both the maximum and minimum porosity of actual granular materials having different gradings and particle aspect ratios.

The densest state is also obtained by gravitational deposition as described in [9,12], but with a contact friction value between particles equal to zero. In fact, setting the friction to zero is favorable for particle rearrangements, which in turn leads to the compaction of the packing [37,43,49]. The minimum porosity reached with such process is equal to that obtained previously by Reboul et al. [28] for the same material (UG) though the process of creation of this dense sample was different. In their work, spheres are initially released under gravity to create a loose sample and then, the densest state is obtained by means of shearing cycles with a contact friction value between particles equal to zero.

It must be noted that such typical DEM densification processes lead to density states which are generally looser than that obtained for actual materials using the ASTM process [5]. Table 1 and Table 2 summarize the

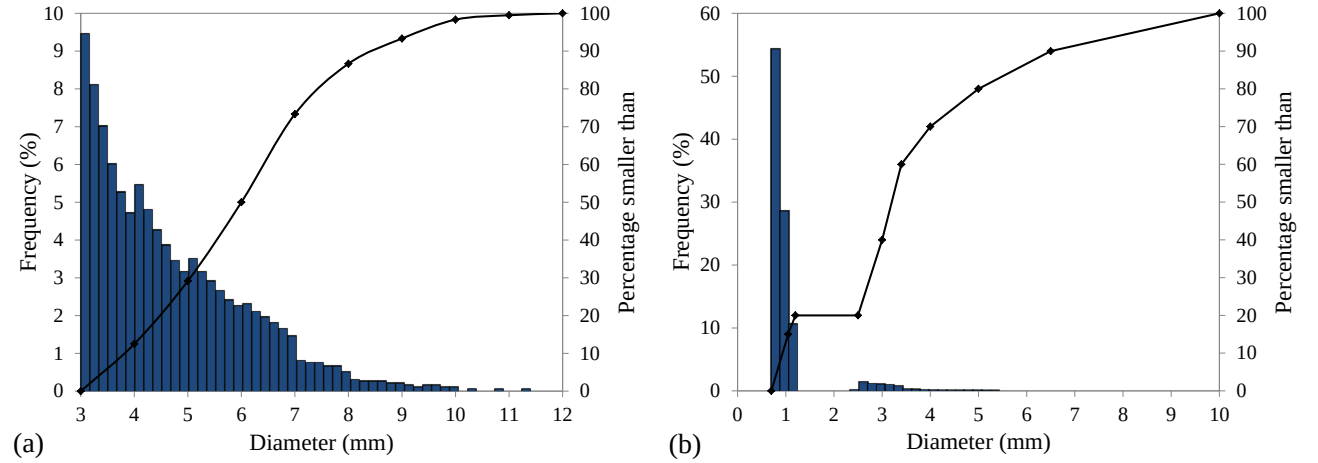

Fig. 4 Particle size distribution (ordinate on the left Y-axis) and cumulative particle size distribution (ordinate on the right Y-axis) for **(a)**: UG material and **(b)**: GG material

set of parameters used to obtain the numerical samples and their induced final properties.

Since the top and bottom boundaries of the sample are not periodic, any computation of the poral characteristics of the packing is carried out within a volume smaller than the total sample volume. While the vertical lateral limits of this measurement volume correspond to the periodic boundaries. The limits of the top and bottom volume exclude then a zone of thickness equal to D_{100} of the granular material. Finally, we checked that the final volume used for the statistics of the void space is greater than the Representative Elementary Volume.

Table 1 Mechanical and numerical parameters for DEM simulations

Parameter	Magnitude
Normal stiffness (K_n)	10^4 KN/m
Tangential stiffness (K_t)	10^4 KN/m
Specific weight of spheres (ρ)	2530 Kg/m^3
Global damping (α)	0.7
Inter-particle friction (μ)	0.3 (loosest state)
	0 (densest state)

Table 2 Characteristics of numerical samples

Material	UG	GG
Coefficient of uniformity (C_u)	1.7	3.6
D_0 - D_{100} (mm)	3 - 12	0.7 - 10
Number of particles	650	25000
Maximum porosity	0.34	0.38
Minimum porosity	0.25	0.34

3 Merging techniques for pores

The generated samples will be used as data basis for the comparison of two different techniques: the overlap of inscribed void spheres and the degree of the separation of pores by their constrictions. Both techniques, without any algorithmic restriction, would produce overmerges in terms of ducts and less interlocked pores. Thus, the techniques are accompanied by algorithmic restriction: the overlapping criterion is based on levels of neighborhood as initially considered by Seblany et al. [33], while the degree of separation is strengthened by a hierarchical separation [18]. Both approaches build data structures from the Delaunay tessellation and the Voronoï decomposition, respectively, and provide tools to extract properties such as pore volumes and constriction sizes.

3.1 Overlapping inscribed void spheres technique

Once the locations and radii of the solid spheres are known, a modified (weighted) tetrahedral tessellation (Delaunay tessellation) of the space is performed [11].

Such a 3D partition induces a specific structure for the pore space. Indeed, each tetrahedron is herein supposed to represent a local pore associated to four exits. The void volume included in each tetrahedron can be derived together with other characteristics including the inscribed void sphere. Then, a statistical study over the whole sample can be computed for the properties of the local pores. Accordingly, constrictions defined as the largest empty discs on the tetrahedron faces can be obtained and the CSD can be deduced by means of a statistical study over the sample. All these characteristics are obtained using optimization algorithms (for the

distance mapping) and more details can be found in [2, 28, 29].

The initial calculation of pores and constrictions corresponds to a level 0 (L_0) of analysis as proposed by Reboul et al. [28]. This direct computation from the Delaunay tessellation can include configurations where constrictions are larger than pores (constrictions formed by non-touching particles on the common face of two adjacent interlocked pores [13]), and other configurations where two adjacent inscribed void spheres are almost superimposed (The overlapping of these void spheres is greater than 99.9999%). Such cases correspond to tetrahedra of undesirable shape (e.g. very flat tetrahedra). The constrictions resulting from these cases represent between 10% to 20% of the total number of constrictions, depending on the grading and on the density of the material. Thus, a L_0 description of the void space may include some artifacts due to the mathematical process used for the partitioning of the space. A post-processing of L_0 (Level $L_0{}'$) guarantees the removal of these degenerated constrictions.

Apart from these cases, the inscribed void spheres of two adjacent tetrahedra may just partly overlap and these cases are distinguished from those where the inscribed void spheres are completely separated. In the case of overlapping, a merging of the corresponding adjacent pores is applied (Fig. 5), giving birth to a level 1 (L_1) characterization of the void space. First, the tetrahedra derived from $L_0{}'$ are sorted by increasing order of their inscribed void sphere, then for each tetrahedron, the overlap criterion is checked for the four adjacent tetrahedra. It should be noted here that after merging two neighboring pores, the process of merging is ended and didn't go beyond the direct neighbor.

A level 2 (L_2) is also processed where merging is not only applied to the adjacent local pore but also to the next adjacent local pore if the inscribed void sphere of this latter overlaps that of the former pore (Fig. 5). No further level for merging pores is envisioned since in that case, the void space will tend to be characterized in terms of duct.

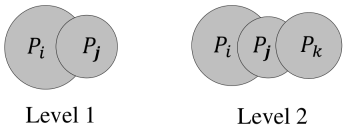

Fig. 5 Definitions of different merging criteria associated to the overlapping inscribed void spheres technique

Level 1 and level 2 can be envisioned as criteria for merging pores in the context of the overlapping inscribed void sphere technique. This technique and the proposed criteria hold some advantages and limits. First, even if this technique seems relevant in the case of packing of spheres where a partition of Delaunay can be processed, it may not be able to address the case of media with elongated particles which may give rise to more elongated pores than in packing of spheres. In that case, by nature, few overlapping inscribed void spheres are expected to be found. In the case of packing of spheres, the proposed two criteria imply that the persistence of a pore is limited in distance which can be both an advantage and a drawback. It implies that a pore can only be defined at a certain local scale involving a pore wall composed of maximum eight particles in the case of L_1 or of tens of particles in the case of L_2.

3.2 Pore separation technique

The pore separation technique relies on the elements of the Voronoï graph that was computed from the spheres geometry based on the Euclidean distance to the solid spheres [20]. As described in Section 1, a Voronoï node P and its respective distance represent a pore and its size d_P in the initial decomposition, and a constriction C with its respective distance describe the narrowest location between two adjacent pores along a Voronoï edge (Fig. 6a).

The separation technique keeps track of this distance information and builds a hierarchical structure of these elements that follows the topology of the distance function. It evaluates the separation of each pair of pores P_i and P_j by their constriction C_{ij} based on the relative diameter difference $t_{\text{diff}}(P_i,C_{ij},P_j) = (d_P - d_{C_{ij}})/d_P$ with $d_P = min(d_{P_i},d_{P_j})$ and $i \neq j$. The value t_{diff} will be used to merge neighboring pores according to the degree of their separation, which is specified by a user-defined threshold t. This approach was initially developed for materials with irregular particles and does not consider sphere overlaps in order to include pairs within elongated pores.

The hierarchical manner arises from specifying tuples $T_{ij} = (P_i,C_{ij},P_j,t_{\text{diff}}(P_i,C_{ij},P_j))$ that are processed in a particular order. The approach starts from tuples of direct neighbors in the unmerged graph (Fig. 6b) and evaluates them in increasing order of the difference thresholds. Each step assigns the smaller pore to the larger one. Hereafter, the neighbor tuples that contain the newly merged pore will be updated by replacing this pore by the larger representative one as well as by re-computing t_{diff} accordingly.

For example, if $d_{P_i} < d_{P_j}$, then all neighbor tuples T_{ik} with $k \neq j$ will be converted to $T_{jk} = (P_j, C_{jk}, P_k, t_{\text{diff}}(P_j,C_{jk},P_k))$ to be neighbors of P_j. P_i and C_{ij} are

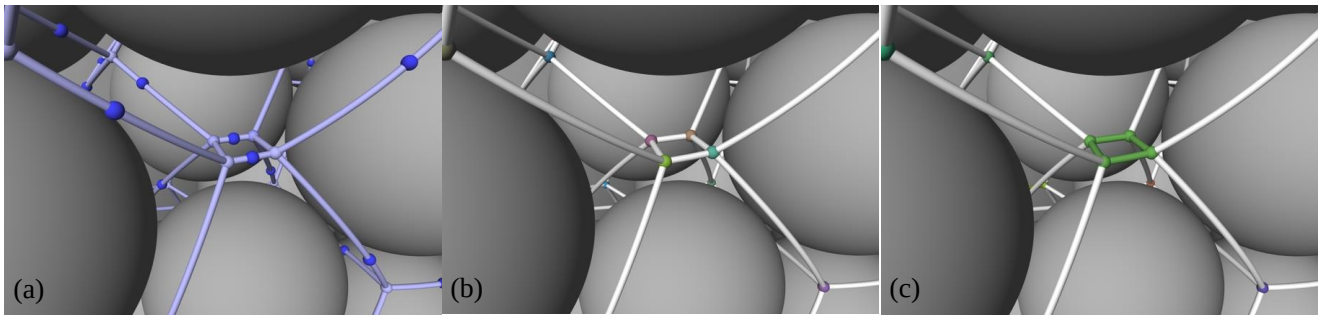

Fig. 6 Detail of spheres and Voronoï graph extracted from the GGD sample; **(a)**: Bright spheres at crossings indicate pore centers, darker spheres indicate constrictions; **(b)**: Unmerged pore centers are randomly colored by their label ID; **(c)**: Merged pore centers and their connection paths and constrictions will be labeled as belonging together ($t = 1\%$)

labeled on the graph as belonging to P_j (Fig. 6c) and will be discarded from further considerations. This step is then repeated until all (newly created) tuples with a difference threshold $t_{\text{diff}} \leq t$ have been processed. More algorithmic details can be found in [18].

The resulting tuples represent hierarchical neighbors rather than direct neighbors, where each pore represents all hierarchically assigned pores. They not only treat local information on the separation but also allow considering the separation between groups of local pores that are less significantly separated. The constriction and the difference relation t_{diff} of such a tuple represent then the most significant separation criterion between the two hierarchically neighbored pores. This can increase their life time as separated pores compared to the direct neighbor relations and avoids inappropriate merge propagation.

Voronoï approaches may produce additional pore centers in the graph that do not correspond to maxima in the distance function. In such cases, the diameter of constriction separating two adjacent pores is equal to that of the smaller pore ($t = 0\%$). This is similar to what was found with the weighted Delaunay tessellation (see Sect. 3.1). On the graph, such constrictions are then identical to the smaller pore (two edges in the center of Fig. 6a), which will be merged at the very beginning of the hierarchical merge.

4 Pore distributions derived from different merging criteria

The dual complexes of the Delaunay/Voronoï decomposition, as already described in Section 1, encode the elements of the pore space of a sphere packing. Herein, the Delaunay cells or tetrahedra are the entities that cover the pores or parts of pores and, thus, the appropriate entity to evaluate the pore volumes from both merging techniques.

4.1 Overlapping inscribed void spheres technique

The computational aspects of Delaunay tessellation involve tetrahedral cells mainly inscribed in the void space, which are more suitable than the Voronoï cells to characterize and quantify pore volumes [7,24].

As explained previously in Section 3.1, the pore size can be measured in terms of the largest inscribed void sphere associated to each tetrahedron but also by considering the sphere having a volume equal to that of the void within a Delaunay cell (L_0) or within merged Delaunay cells (L_1, L_2). This latter method is denoted in the following *equivalent void sphere* approach. Using these two definitions for characterizing the pores, the distribution of pore sizes, for UG and GG materials, at loose and dense states, are plotted in Figure 7 and Figure 8. It is interesting to note that the pore size distributions can be well described by a Log-Normal law in agreement with previous studies [28,48]. The correlation is almost perfect for L_0 (not shown herein); nevertheless, the statistical model tends to shift the mode towards larger pore diameters and to attenuate its frequency when L_1 and L_2 criteria are considered.

For UGL sample, accordingly to the work of Reboul et al. [28] on the same grading, the distribution computed on the basis of the inscribed void spheres approach has a mode shifted towards the smaller diameters compared to the other distributions obtained by the equivalent void sphere approach, since this former approach disregards a part of the void space. Moreover, the distribution obtained from L_1 is quite different than that corresponding to L_0, and a slight decrease in the modal value is also observed, thus showing that numerous pores around the mode in L_0 have been merged in L_1. On the contrary, no significant difference in the equivalent pore diameter distribution is observed from L_1 to L_2 (Fig. 7a). It tends to indicate that within the framework of this merging technique, the persistence of

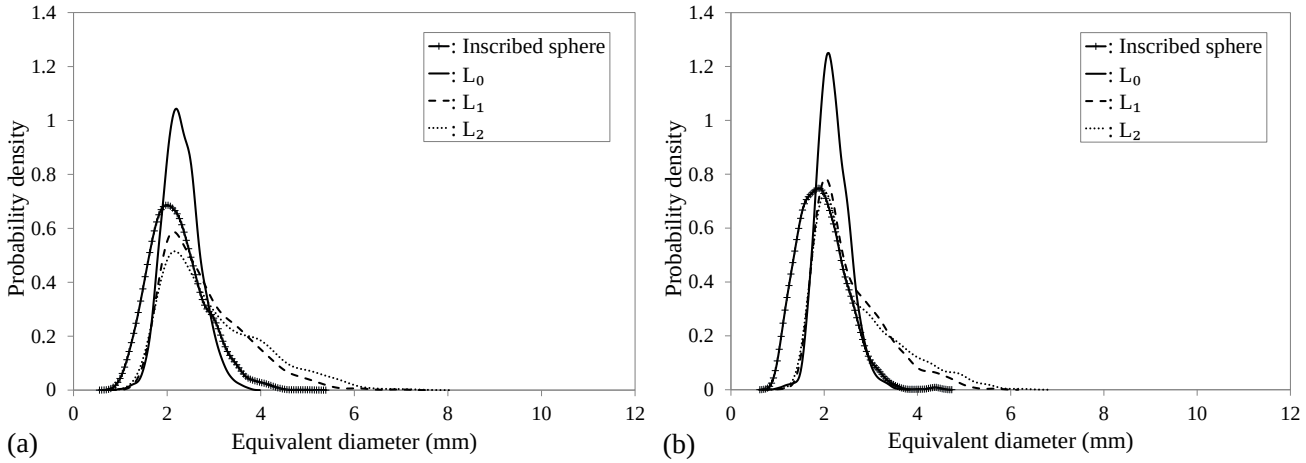

Fig. 7 Probability density functions for the equivalent pore diameter resulting from different definitions and corresponding to the overlapping inscribed void spheres technique; **(a)**: UGL, **(b)**: UGD

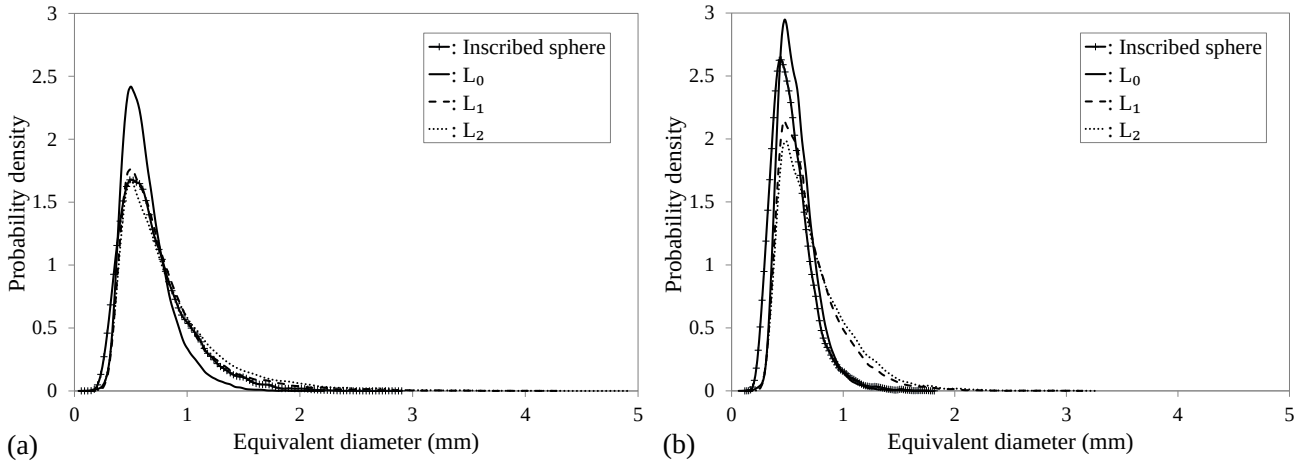

Fig. 8 Probability density functions for the equivalent pore diameter resulting from different definitions and corresponding to the overlapping inscribed void spheres technique; **(a)**: GGL, **(b)**: GGD

a pore is mainly limited to an adjacent tetrahedron for a given Delaunay cell.

For GGL sample, the distribution and the modal value corresponding to the inscribed void sphere are only slightly shifted towards the smaller diameters. This may be a consequence of the wide range of particle sizes involved in this material, which tends to generate more flat tetrahedra with inscribed void spheres which are not entirely confined in these tetrahedra. Consequently, this would create the possibility of greater void spheres than in the case of UG material, the volume of which could match the volume of L_1 or L_2 distribution (Fig. 8a). It must be noted that other well graded materials that were studied (not shown herein) also exhibited this pattern. However, the tetrahedral shape seems to be the main configuration represented within the sample, irrespective of the grading and porosity, since the modal values for L_0, L_1 and L_2 are almost similar. The same finding was observed by Reboul et al. [28] for UGL sample.

For the densest states (Fig. 7b and Fig. 8b), as expected, the equivalent diameter distributions are narrower than those resulting from the loosest state (Fig. 7a and Fig. 8a); this is also accompanied by a decrease of the modal values. In fact, during the process of densification, all the pores tend to reduce their volumes but the larger ones are more sensitive to this process. Indeed, arching that allows larger pores to be created in UGL and GGL samples tends to be destroyed due to the reduction of the local friction ratio during the process of densification.

Figure 9 shows the number of Delaunay cells per pore in the case of L_1, for UG and GG materials, at loose and dense states. Irrespective of the porosity and of the grading, about 50% of Delaunay cells are not affected by the merging. The tetrahedral shape is then predominant, while more complex entities involving three

or four tetrahedra (sharing a common face with a central tetrahedron) are poorly represented in the sample.

4.2 Pore separation technique

As outlined previously, the pore separation technique is based on the pore-constriction size relations extracted from a Voronoï graph [20]. It computes the Voronoï nodes by determining their four generator spheres, which also are the spheres that build the corresponding tetrahedra in the Delaunay tessellation.

To measure the pore sizes for the comparison, an approximated method was applied to each tetrahedron and its bounding box. A set of quasi-random points (obtained from a Niederreiter sequence [25]) were spatially distributed within the bounding box. Knowing the volume of the bounding box, the void volume is estimated from the number of void points (points located inside the tetrahedron but outside the spherical particles) compared to the number of total points.

The underlying equivalent pore size distributions are given in Figure 10 for both UGL and GGL samples, and similar observations can be reported when the inscribed void sphere distribution is compared to that derived from L_0 (unmerged cells). Additionally, Figure 10 shows the behavior for large thresholds ($t = 30\%$): the difference between the equivalent pore size distributions become highly significant. The mode is very shifted towards the larger diameters. Such a large threshold merges pore clusters that already had been merged for smaller thresholds and, thus, massively increases the corresponding pore size.

4.3 Discussion

A comparison of the pore distributions associated to different merging criteria is developed in this section. As expected, the distributions of the inscribed void sphere diameter provided by the two tessellations of the void space are identical (Fig. 7a and Fig. 10a; Fig. 8a and Fig. 10b). The equivalent diameter of pores in the Delaunay cells derived from L_0 computation in both approaches was found quite similar which was also expected.

A correspondence between different merging criteria in terms of pore size distribution is given in Table 3 and Table 4, for respectively UG and GG materials, at loose and dense states. It can be seen from Table 3 that the minimum relative errors, for UG material, correspond to the couple L_1 and $t = 2\%$ as well as L_2 and $t = 5\%$ independently of the density. Similarly, Table 4 shows

Table 3 Relative error (in %) between the pore size distributions derived from different merging criteria for UG

	$t(\%)$	1	2	3	4	5	6
UGL	L_1	3.9	3.0	3.1	3.8	5.6	8.2
	L_2	9.0	6.5	4.6	2.5	1.7	2.3
UGD	L_1	3.7	2.1	2.2	2.8	4.2	5.5
	L_2	7.5	5.6	3.9	1.8	1.0	1.2

Table 4 Relative error (in %) between the pore size distributions derived from different merging criteria for GG

	$t(\%)$	1	2	3	4	5	6
GGL	L_1	2.5	5.5	8.2	11.1	13.7	16.4
	L_2	5.5	3.4	3.2	5.5	7.8	10.2
GGD	L_1	3.5	2.2	3.0	4.7	6.4	8.1
	L_2	6.3	4.3	3.1	2.2	2.4	4.0

that the equivalent pore distribution corresponding to L_1 is close to that derived from $t = 1\%$, while the equivalent pore distribution derived from L_2 is closer to that resulting from $t = 3\%$. For GGD sample, the minimum relative error is found at $t = 2\%$ ($t = 4\%$ respectively) for L_1 (L_2 respectively).

For UG material, higher values of t are required to generate pore distributions similar to those obtained by the overlapping inscribed void spheres approach. This discrepancy is most likely caused by the nature of the pore network of the studied materials. Broadly graded material, notably at loosest state, more frequently produce clusters of dense inscribed spheres with large overlap, whereas inscribed spheres seem to be more distant with smaller overlap (higher separation) in the UG material. Furthermore, within broadly graded material, several solid spheres may build large voids containing large clusters of inscribed spheres. Such cases may exceed the expected maximum size given by the neighbor levels in the overlapping spheres approach and produce multiple pore instances within such a void. Late merges during the separation merge in UG material and underestimated volumes in GG during the L_1 and L_2 merges most likely lead to the drifting of the L_1 - t and L_2 - t correspondences between the UG and GG materials.

Each technique holds its own limits and holds some advantages. The overlapping inscribed void spheres approach provides a pre-defined neighborhood limit (L_1 and L_2) assuming a general maximum pore size at a meso scale. It may be artificial but seems relevant for packing of spheres. Nevertheless, in the case of granular materials with elongated particles, this technique may not be appropriate since one expects to find elongated pores with scarce overlapping inscribed void spheres occurrences. The separation technique allows tuning the

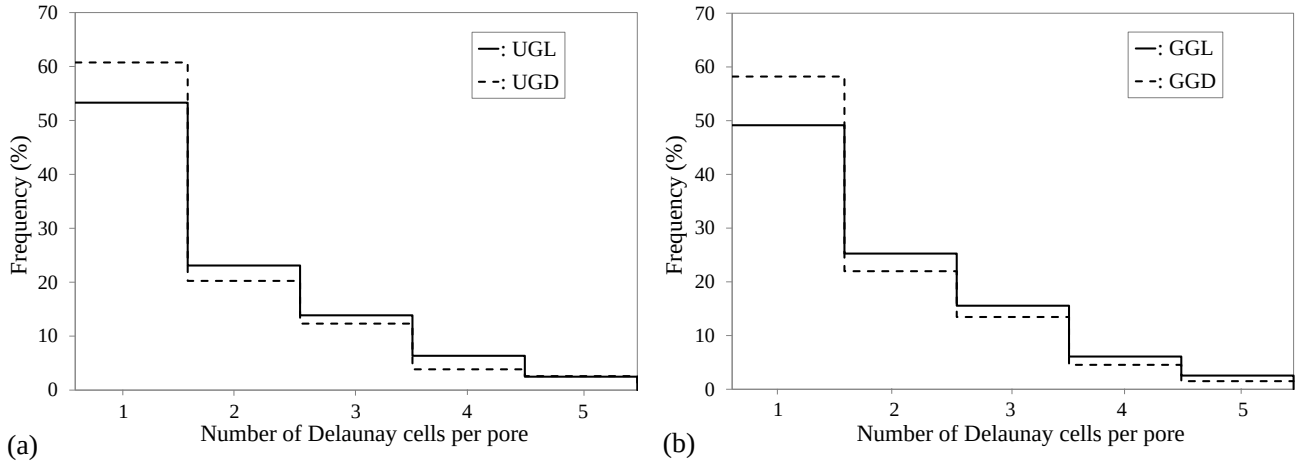

Fig. 9 Number of Delaunay cells per pore in L_1 for loose and dense states; **(a)**: UG, **(b)**: GG

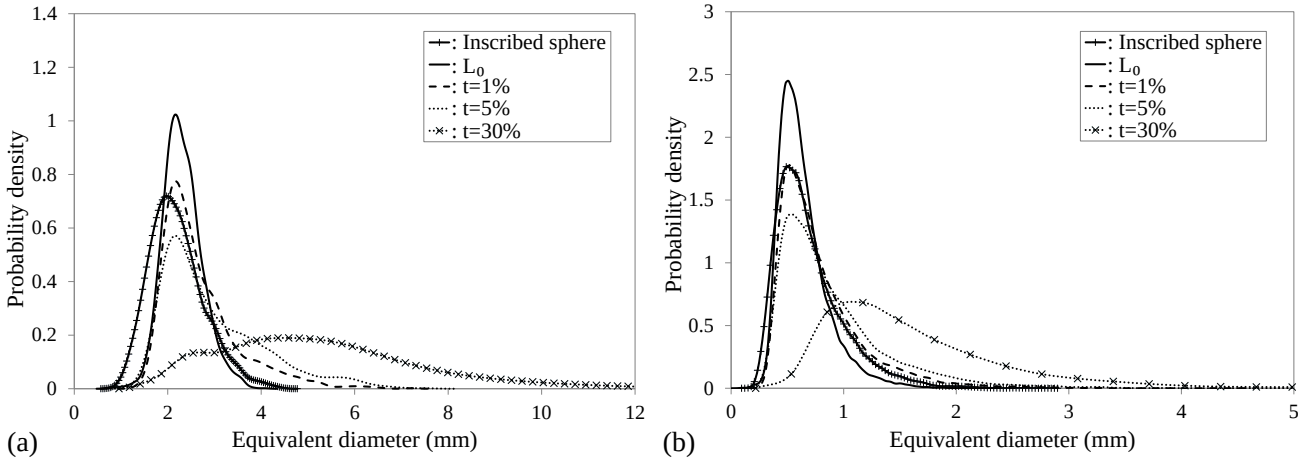

Fig. 10 Probability density functions for the equivalent pore diameter resulting from different definitions and corresponding to the pore separation technique; **(a)**: UGL, **(b)**: GGL

pore structure more easily but the definition of the threshold is difficult and requires experience. One can note that this technique is more robust since it can be used for any granular material with any particle shape if a voxelization representation of the material (solids and voids) is available.

5 Constriction size distributions derived from different merging criteria

For convenience purposes, only the results corresponding to the UGL and GGL samples are presented in this section, but similar results were also found for UGD and GGD samples.

5.1 Overlapping inscribed void spheres technique

The CSDs and the estimated probability density of constriction sizes for L_1 and L_2 merging are given in Figure 11 and Figure 12 for both samples.

First, it has been noted that the number of constrictions decreases by approximately 40% from L_0 to L_1. In fact, the initial computation (L_0) involves non negligible sets of tetrahedra with overlapping inscribed void spheres that are merged in L_1. About half of them comes from odd configurations (that were removed in $L_0{}'$ merging as described in Section 3.1), the other half comes from partly overlapping inscribed void spheres. Moreover, L_2 merging just provides few further merged pores than L_1 which means that such cases are not significantly present in the packing of spheres. Accordingly, a shift towards smaller constriction sizes is reported when comparing L_1 CSD with L_0 CSD (Fig. 11a and Fig. 12a).

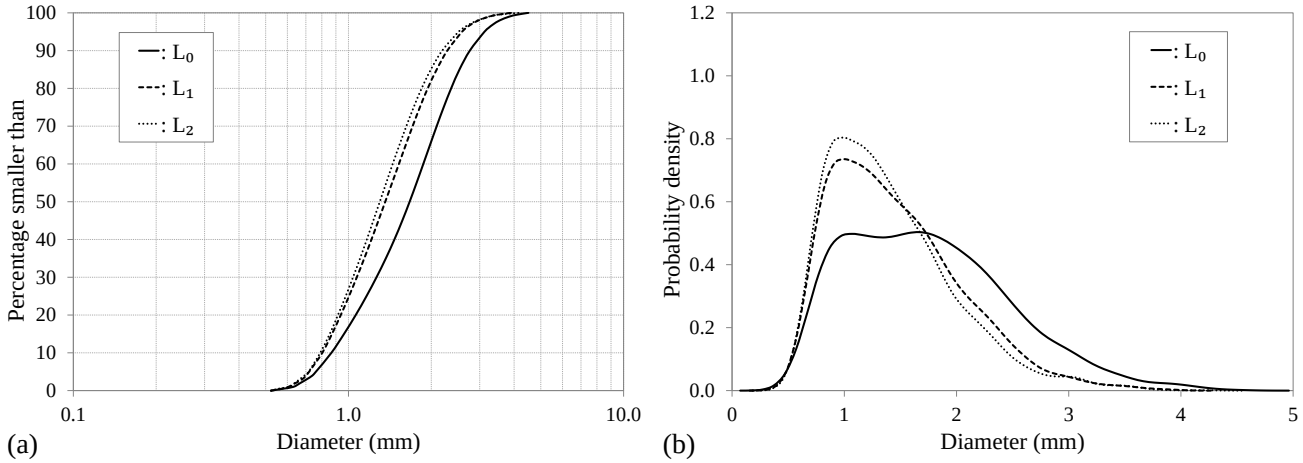

Fig. 11 **(a)**: CSDs for the UGL sample; **(b)**: underlying probability density function for different merging criteria defined in the overlapping inscribed void spheres technique

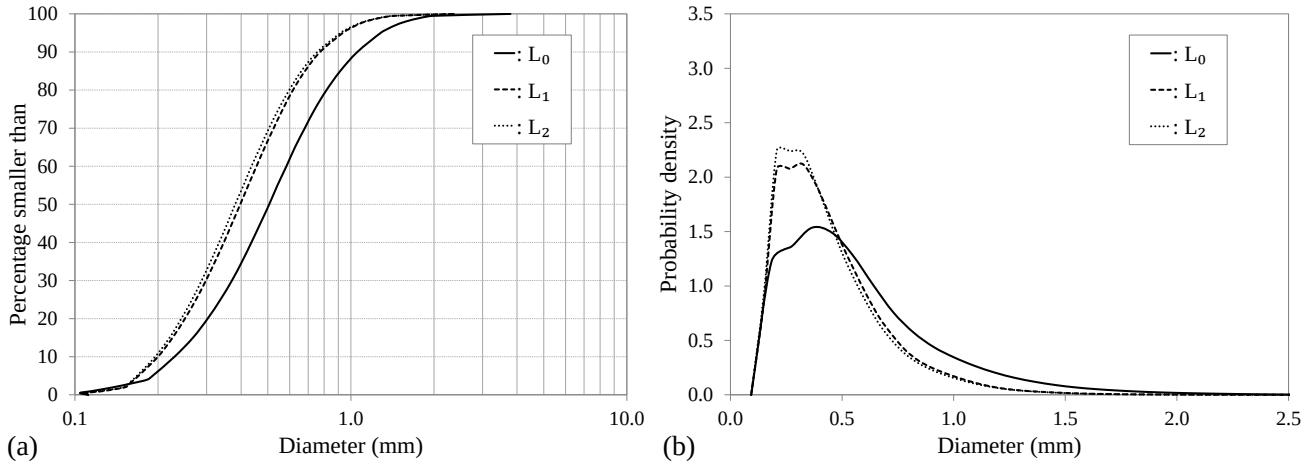

Fig. 12 **(a)**: CSDs for the GGL sample; **(b)**: underlying probability density function for different merging criteria defined in the overlapping inscribed void spheres technique

Indeed, further merging criteria belonging to L_1 were also studied [33]. In addition to the overlap condition, these criteria (herein denoted $L_1(p\%)$, p is the threshold denoted as t in the pore separation technique) evaluate the degree of separation between pores (see Sect. 3.2). The evolution of the relative number of constrictions corresponding to UG and GG materials, at loose and dense states, is shown in Figure 13. It can be noted that the configurations involving a low degree of separation (more precisely $p \leq 10\%$) are more represented within the samples. Furthermore, the decrease in the number of remaining constrictions is most significant in the case of GG material (Fig. 13b) and at loosest state in general.

Another feature is observed in Figure 11b. Merging tends to let appear a clear and single mode while vanishing a coupled second mode. When merging, the first mode for the constriction size almost stabilizes irrespective of the merging level (L_1, L_2). According to Yang et al. [48], the first mode corresponds to the constriction formed by nearly contacting particles while the second one corresponds to that formed by non-touching particles. By merging interlocked pores, the constrictions formed on the common face of the tetrahedra associated to these pores are eliminated, and consequently, the first mode becomes more significant. It must be noted that the CSD, for dense packing, has a strong first mode and a rather weak second mode since, in this case, the Delaunay cells are mainly formed by touching particles.

For GGL, the distribution of constriction sizes exhibits also two distinct modes. In contrast to UGL, the distribution resulting from L_1 or L_2 remains bimodal (Fig. 12b). In such a case, the smaller mode which is approximately not affected by the merging is probably related to constrictions between fine particles in contact while the large one may include constrictions involving at least one particle of diameter greater than

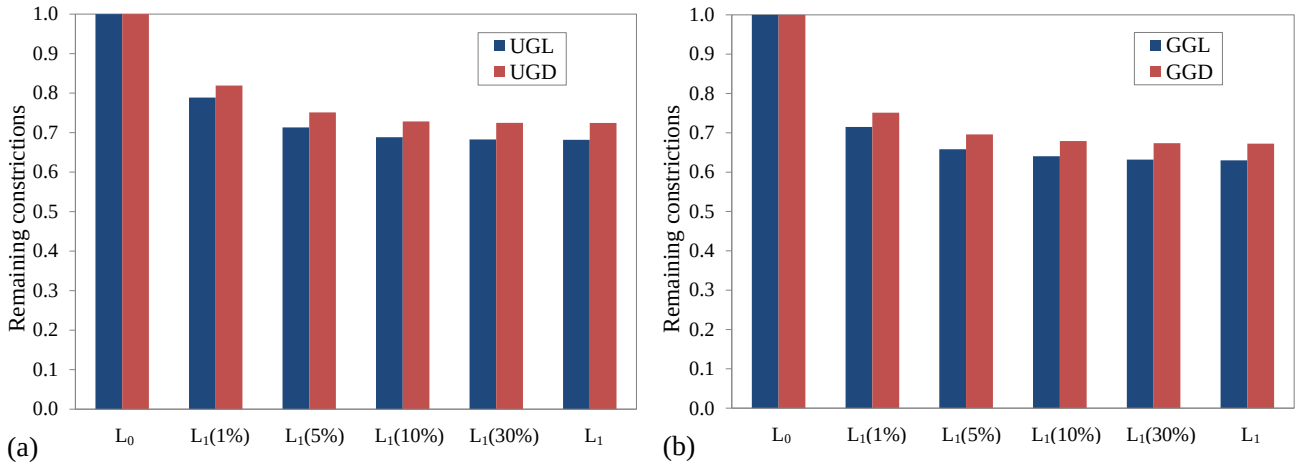

Fig. 13 Evolution of the relative number of constrictions for different merging criteria belonging to L_1, at loose and dense states; **(a)**: UG, **(b)**: GG

the gap. Therefore, the second mode is not destroyed when merging.

Another reason behind can be the large clusters exceeding the L_1 and L_2 neighborhood levels in the GG material as described in Section 4.3. Multiple L_1 or L_2 instances are created within such a void while keeping relatively large constrictions connecting these instances.

In general, from the initial set of constrictions, irrespective of the grading, more than 60% of them correspond to the exits of a single Delaunay cell and about 40% were removed from the statistics by the used merging criteria, which is significant.

5.2 Pore separation technique

Figure 14 and Figure 15 show the CSDs and the estimated probability density of constriction sizes for respectively UGL and GGL samples. One can note that the CSDs gradually shift towards the smaller diameters as the threshold value t increases, and this is accompanied by a progressive decrease in the number of constrictions. Small thresholds mainly merge larger constrictions between pores within voids, which are bounded by smaller constrictions that connect these void clusters. The hierarchical approach strengthens the separation value for the latter ones so that they persist longer. Large thresholds will also merge these cluster-connecting constrictions successively so that the deduced pore structure is highly affected as shown for $t = 30\%$, which can certainly be considered as a significant separation (Fig. 14a and Fig. 15a).

In the case of UGL, the probability density of constriction sizes has two modes for L_0, and then becomes unimodal when merging criteria are applied (Fig. 14b). Besides, the first mode is not affected by the merging steps for t lower than 5%.

For GGL, the L_0 probability density (Fig. 15b) is similar to that obtained in Figure 12b but the bimodal character is not as pronounced. However, the distributions still exhibit a bimodal shape when merging, as described in Section 5.1.

5.3 Discussion

It has been proven in a previous study involving UGL sample that the initial L_0 CSDs derived from the Delaunay and the Voronoï methods are almost congruent [44]. Herein, the proof is also given for the studied GGL sample (Fig. 16) even if it was expected.

The two different merge approaches are based on completely different techniques: overlapping spheres in a local manner and the pore separation in a hierarchical sense. This may lead to different merge behavior.

The overlapping inscribed void spheres approach implies a criterion based on the distance between the centers of adjacent pores which seems to be more reasonable according to Al-Raoush et al. [2] where neighboring pores are merged if the center of an inscribed void sphere lies within the adjacent inscribed void sphere. In fact, a statistical study over all tuples (P_i, C_{ij}, P_j) shows that more than 50% of overlap cases fulfil Al-Raoush et al. criterion and thus correspond to highly interconnected pores.

The separation technique evaluates the importance of the distance maxima and minima along the Voronoï graph: it fuses local pores that are insignificantly separated to their next larger pore, then evaluates the remaining more important pores among each other building up a hierarchy. That way, it detects significant con-

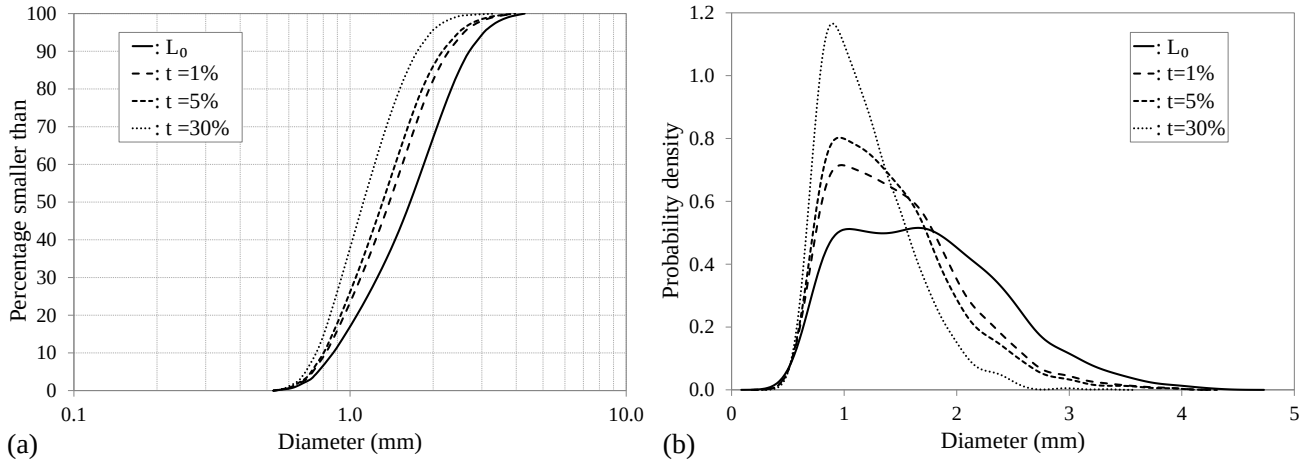

Fig. 14 **(a)**: CSDs for the UGL sample; **(b)**: underlying probability density function of the constriction diameter for different merging steps associated to the pore separation technique

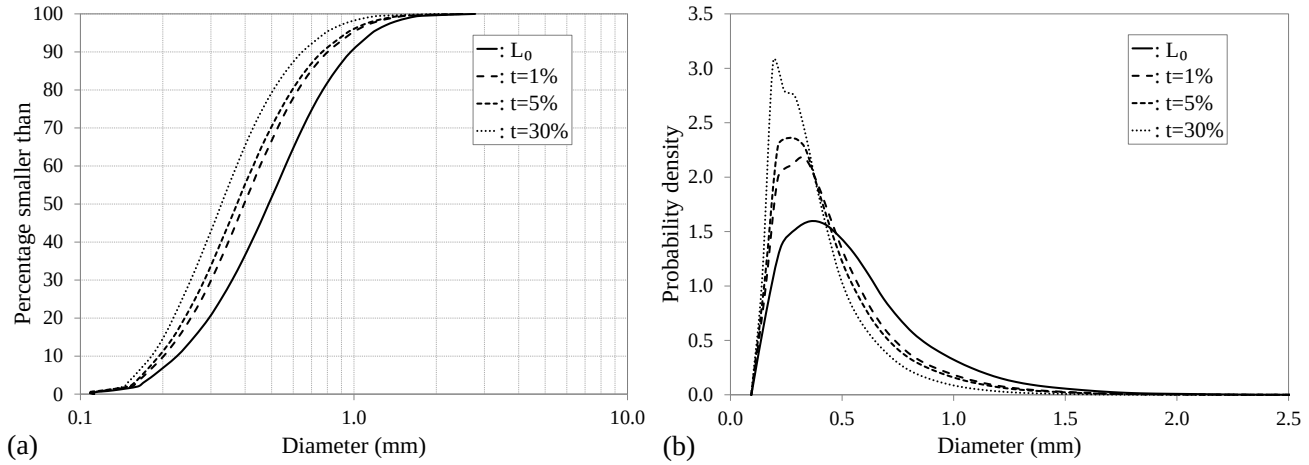

Fig. 15 **(a)**: CSDs for the GGL sample; **(b)**: underlying probability density function of the constriction diameter for different merging steps associated to the pore separation technique

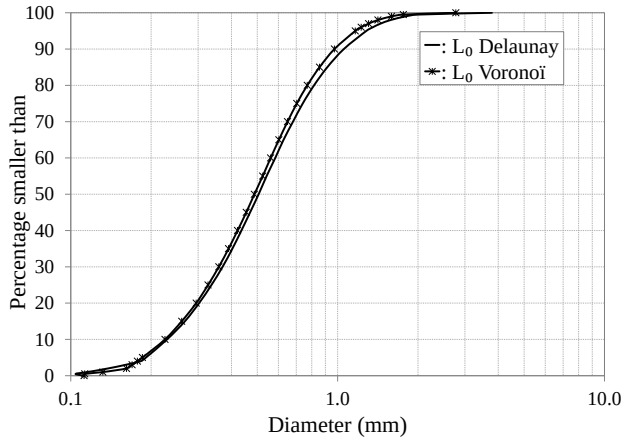

Fig. 16 Initial CSD derived from Delaunay and Voronoï approaches for GGL sample

strictions and stops merging there for a given hierarchy level, which depends on a user-defined threshold.

For each material, the relative error between the CSDs derived from different merging criteria is calculated and given in Table 5 and Table 6. For UG material, the correspondence between the two merging techniques, previously found for the pore distribution, hold true for the CSD (L_1 and $t = 2\%$; L_2 and $t = 5\%$) (Tab. 5). For GGL sample, Table 6 indicates that the resulting CSDs provided by L_1 and L_2 are closer to those derived from $t = 1\%$ and $t = 4\%$ respectively. Furthermore, one can note that, for the densest state, the CSD associated to L_1 and that corresponding to $t = 2\%$ are approximately similar and it seems that a threshold value of 5% is more suitable to predict L_2. Nevertheless, satisfactory results can be obtained between $t = 1\%$ and $t = 2\%$ for L_1, and over the range of $4-6\%$ for L_2. More precisely, and irrespectively of density and grading, a threshold of about 2% (5% respectively) can be considered suitable to predict the

pore and constriction size distributions corresponding to L_1 (L_2 respectively).

Table 5 Relative error (in %) between the CSD derived from different merging criteria for UG

	$t(\%)$	1	2	3	4	5	6
UGL	L_1	1.4	1.2	1.7	2.3	3.0	3.7
	L_2	4.2	3.1	2.4	1.8	1.4	1.5
UGD	L_1	2.2	2.0	2.3	3.2	4.0	4.8
	L_2	4.8	3.5	2.8	2.0	1.7	1.9

Table 6 Relative error (in %) between the CSD derived from different merging criteria for GG

	$t(\%)$	1	2	3	4	5	6
	$t(\%)$	1	2	3	4	5	6
GGL	L_1	2.1	2.1	2.6	3.0	3.6	4.0
	L_2	4.6	3.0	1.9	1.5	1.8	2.1
GGD	L_1	2.2	0.9	1.0	1.7	2.5	3.4
	L_2	4.6	2.9	1.7	0.9	0.8	1.5

6 Conclusion

In this paper, different void characteristics in packings of spheres are derived from a partition of the space. These characteristics are the distribution of the diameter of the void sphere having a volume equal to that of the pore, which characterizes the morphology of the void space, and the constriction size distribution which characterizes its topology. Since the usual Delaunay or Voronoï partitions may lead to an artificial oversegmentation of the pore space, two different techniques for merging local pores were studied and compared. These techniques, which lie on the computation of the inscribed void sphere associated to a local pore, are the overlapping void spheres technique and the pore separation technique.

In the overlapping void spheres approach, two criteria or levels are defined: a level 1 (L_1) where two direct neighboring local pores are merged if their respective inscribed void spheres are overlapping, and a second level (L_2), where the next neighboring local pores can also be merged with the two first ones to create a single pore in case of further overlapping of void inscribed spheres. The pore separation technique hierarchically evaluates the degree of separation indicated by the distance function of the void space for a given threshold t. To compare both approaches, different thresholds t were tested to show the impact of the merging criterion on the distribution of pore and constriction sizes.

Two materials were studied, one which can be considered as uniformly graded and another one which is widely graded but gap-graded, both in a loose or in a dense state. From a direct computation of pores and constrictions, L_1 merging induces the removal of about 40% of constrictions irrespective of the grading and of the density. L_2 level merging brings fewer new merging of local pores. In the pore separation technique, the removal of constrictions is important for small values of the threshold ($t \leq 1\%$) irrespective of grading and density, and the rate of removal of further constrictions tends to decrease as t increases.

In the case of the uniformly graded material, merging tends to remove the larger constrictions and lets appear a clear single mode for the distributions of constriction sizes. In the case of the studied gap-graded material, two close modes are obtained after merging which is just typical of the studied grading. The same trend is observed with the pore separation technique while t is equal or smaller than 5%. For larger threshold values, the constriction size corresponding to the mode tends to shift to the smaller diameters.

A correspondence is found between the two merging techniques irrespective of the considered void characteristics, pores or constrictions, the grading and the density. L_1 merging corresponds to a threshold of about 2% and L_2 to a threshold of about 5%. It can serve as a guide for a user for the definition of pores at a meso scale even if a definite pore structure cannot be obtained due to subjective nature of these bodies.

Acknowledgements Part of this work belongs to a project funded by *Compagnie Nationale du Rhône* (CNR). F. Seblany and E. Vincens acknowledge CNR for its interest and its financial support.

References

1. Allen, M. P., Wilson, M. R.: Computer simulation of liquid crystals. Journal of Computer-Aided Molecular Design **3**(4), 335–353 (1989)
2. Al-Raoush, R., Thompson, K., Willson, C.S.: Comparison of network generation techniques for unconsolidated porous media. Soil Science Society of America Journal **67**(6), 1687–1700 (2003)
3. Barreto Gonzalez, D.: Numerical and experimental investigation into the behaviour of granular materials under generalised stress states. Doctoral Dissertation, Imperial College London (2010)
4. Benahmed, N., Canou, J., Dupla, J. C.: Structure initiale et propriétés de liquéfaction statique d'un sable. Comptes Rendus Mécanique **332**(11), 887–894 (2004)
5. Bernhardt, M. L., Biscontin, G.: Experimental validation study of 3D direct simple shear DEM simulations. Soils and Foundations **56**(3), 336–347 (2016)

6. Biarez, J., Hicher, P.Y.: Classification of and correlations between parameters from Elementary Mechanics of Soil Behavior. A.A. Balkema, Rotterdam, 81–106 (1994)
7. Bryant, S. L., King, P. R., Mellor, D. W.: Network model evaluation of permeability and spatial correlation in a real random sphere packing. Transport in Porous Media **11**(1), 53–70 (1993)
8. Chareyre, B., Cortis, A., Catalano, E., Barthlemy, E.: Pore-scale modeling of viscous flow and induced forces in dense sphere packings. Transport in Porous Media **94**(2), 595–615 (2012)
9. Cui, L., O'Sullivan, C.: Analysis of a triangulation based approach for specimen generation for discrete element simulations. Granular Matter **5**(3), 135–145 (2003)
10. Cundall, P. A., Strack, O. D.: A discrete numerical model for granular assemblies. Geotechnique **29**(1), 47–65 (1979)
11. Edelsbrunner, H., Shah, N. R.: Incremental topological flipping works for regular triangulations. Algorithmica **15**(3), 223–241 (1996)
12. Feng, Y.T., Owen, D.R.J.: Filling domains with disks: an advancing front approach. International Journal for Numerical Methods in Engineering **56**(5), 699–713 (2003)
13. Gao, S., Meegoda, J. N., Hu, L.: Two methods for pore network of porous media. International Journal for Numerical and Analytical Methods in Geomechanics **36**(18), 1954–1970 (2012)
14. Gervois, A., Oger, L., Richard, P., Troadec, J. P.: Voronoï and radical tessellations of packings of spheres. In: International Conference on Computational Science, 95–104. Springer (2002)
15. Giesche, H.: Mercury porosimetry: a general (practical) overview. Particle & Particle Systems Characterization **23**(1), 9–19 (2006)
16. Gladkikh, M., Bryant, S.: Prediction of imbibition in unconsolidated granular materials. Journal of Colloid and Interface Science **288**(2), 526–539 (2005)
17. Homberg, U., Baum, D., Prohaska, S., Kalbe, U., Witt, K.J.: Automatic extraction and analysis of realistic pore structures from μCT data for pore space characterization of graded soil. In: Proceedings of the 6th International Conference Scour and Erosion (ICSE-6), 66–73 (2012)
18. Homberg, U., Baum, D., Wiebel, A., Prohaska, S., Hege, H.C.: Definition, extraction, and validation of pore structures in porous materials. In: Topological Methods in Data Analysis and Visualization III, 235–248. Springer (2014)
19. Kenney, T., Chahal, R., Chiu, E., Ofoegbu, G., Omange, G., Ume, C.: Controlling constriction sizes of granular filters. Canadian Geotechnical Journal **22**(1), 32–43 (1985)
20. Lindow, N., Baum, D., Hege, H. C.: Voronoï-based extraction and visualization of molecular paths. IEEE Transactions on Visualization and Computer Graphics **17**(12), 2025–2034 (2011)
21. Locke, M., Indraratna, B.: A new model for the behaviour of granular filters. In: Proceedings of the Fourth Australia New Zealand Young Geotechnical Professionals Conference. University of Western Australia 147 (2000)
22. Locke, M., Indraratna, B., Adikari, G.: Time-dependent particle transport through granular filters. Journal of Geotechnical and Geoenvironmental Engineering **127**(6), 521–529 (2001)
23. Mason, G., Mellor, D. W.: Simulation of drainage and imbibition in a random packing of equal spheres. Journal of Colloid and Interface Science **176**(1), 214–225 (1995)
24. Mellor, D. W.: Random close packing (RCP) of equal spheres: structure and implications for use as a model porous medium. Doctoral Dissertation, Open University (1989)
25. Niederreiter, H.: Low-discrepancy and low-dispersion sequences. Journal of Number Theory **30**(1), 51–70 (1988)
26. O'Sullivan, C., Bluthé, J., Sejpar, K., Shire, T., Cheung, L. Y. G.: Contact based void partitioning to assess filtration properties in DEM simulations. Computers and Geotechnics **64**, 120–131 (2015)
27. Radjai, F., Voivret, C.: Periodic boundary conditions. Discrete Numerical Modeling of Granular Materials, 181–198 (2011)
28. Reboul, N., Vincens, E., Cambou, B.: A statistical analysis of void size distribution in a simulated narrowly graded packing of spheres. Granular Matter **10**(6),457–468 (2008)
29. Reboul, N., Vincens, E., Cambou, B.: A computational procedure to assess the distribution of constriction sizes for an assembly of spheres. Computers and Geotechnics **37**(1), 195–206 (2010)
30. Richard, P., Oger, L., Troadec, J. P., Gervois, A.: Tessellation of binary assemblies of spheres. Physica A: Statistical Mechanics and its Applications **259**(1), 205–221 (1998)
31. Roux, J. N., Chevoir, F.: Simulation numérique discrete et comportement mécanique des matériaux granulaires. Bulletin des Laboratoires des Ponts et Chaussées **254**, 109 (2005)
32. Schuler, U.: Scattering of the composition of soils. An aspect for the stability of granular filters. In: Geofilters **96**, 21–34 (1996)
33. Seblany, F., Homberg, U., Vincens, E., Winkler, P., Witt, K. J.: Merging criteria for the definition of a local pore and the CSD computation of granular materials. In: Proceedings of the 25th Meeting of European Working Group on Internal Erosion (EWGIE). Delft, 150–159 (2017)
34. Shire, T., O'Sullivan, C.: A network model to assess base-filter combinations. Computers and Geotechnics **84**, 117–128 (2017)
35. Silveira, A.: An analysis of the problem of washing through in protective filters. In: Proceedings of the 6th International Conference on Soil Mechanics and Foundation Engineering. Montréal, Que 551–555 (1965)
36. Silveira, A., de Lorena Peixoto, T., Nogueira, J.: On void size distribution of granular materials. In: Proceedings of the 5th Pan American Conference on Soil Mechanics and Foundation Engineering. Buenos Aires, 161–177 (1975)
37. Sitharam, T.G., Dinesh, S.V., Shimizu, N.: Micromechanical modelling of monotonic drained and undrained shear behaviour of granular media using three-dimensional DEM. International Journal for Numerical and Analytical Methods in Geomechanics **26**(12), 1167–1189 (2002)
38. Sjah, J., Vincens, E.: Determination of the constriction size distribution of granular filters by filtration tests. International Journal for Numerical and Analytical Methods in Geomechanics **37**(10), 1231–1246 (2013)
39. Šmilauer, V., Catalano, E., Chareyre, B., Dorofeenko, S., Duriez, J., Gladky, A., Kozicki, J., Modenese, C., Scholtès, L., Sibille, L., Stránský, J., Thoeni, K.: Yade Documentation. V. Šmilauer ed. (2010)
40. Soria, M., Aramaki, R., Viviani, E.: Experimental determination of void size curves from Filters. Geotechnical and Hydraulic Engineering, 43–48 (1993)
41. Sufian, A., Russell, A. R., Whittle, A. J., Saadatfar, M.: Pore shapes, volume distribution and orientations in monodisperse granular assemblies. Granular Matter **17**(6), 727–742 (2015)
42. Thommes, M.: Physical adsorption characterization of nanoporous materials. Chemie Ingenieur Technik **82**(7), 1059–1073 (2010)
43. Thornton, C.: Numerical simulations of deviatoric shear deformation of granular media. Géotechnique **50**(1), 43–53 (2000)

44. Vincens E., Witt K.J., Homberg U.: Approaches to determine the Constriction Size Distribution for understanding filtration phenomena in granular materials. Acta Geotechnica **10**(3), 291–303 (2015)
45. Vogel, H. J., Roth, K.: Quantitative morphology and network representation of soil pore structure. Advances in Water Resources **24**(3), 233–242 (2001)
46. Witt, K.J.: Filtrationsverhalten und Bemessung von Erdstoff-Filtern. Institut für Bodenmechanik und Felsmechanik der Universität Fridericiana in Karlsruhe **104** (1986)
47. Yang, R. Y., Zou, R. P., Yu, A. B.: Voronoï tessellation of the packing of fine uniform spheres. Physical Review E **65**(4), 041302 (2002)
48. Yang, R.Y., Zou, R.P., Yu, A.B., Choi, S.K.: Pore structure of the packing of fine particles. Journal of Colloid and Interface Science **299**(2), 719–725 (2006)
49. Zhang, Z. P., Liu, L. F., Yuan, Y. D., Yu, A. B.: A simulation study of the effects of dynamic variables on the packing of spheres. Powder Technology **116**(1), 23–32 (2001)